Chemical Engineering Journal 503 (2025) 157894

Contents lists available at ScienceDirect

Chemical Engineering Journal

journal homepage: www.elsevier.com/locate/cej

Assessment of solar photocatalytic wastewater disinfection and microcontaminants removal by modified-allophane nanoclays based on TiO_2, Fe and ZnO at laboratory and pilot scale

Jorge Castro-Rojas [a,b,c,d], Maria A. Rao [b], Ilaria Berruti [e,f], Maria Luz Mora [c,g], Elizabeth Garrido-Ramírez [d,h], María Inmaculada Polo-López [e,f,*]

[a] Programa de Doctorado en Ciencias de Recursos Naturales, Universidad de La Frontera, Av. Francisco Salazar 01145, PO Box 54-D Temuco, Chile
[b] Dipartimento di Agraria, Università degli Studi di Napoli Federico II, via Università 100, Portici 80055, Italy
[c] Departamento de Ciencias Químicas y Recursos Naturales, Universidad de la Frontera, Av. Francisco Salazar 01145, PO Box 54-D Temuco, Chile
[d] Escuela de Ciencias Ambientales y Sustentabilidad, Universidad Andres Bello, República 440, Santiago 83270255, Chile
[e] CIEMAT-Plataforma Solar de Almería, Carretera Senés, Km 4, 04200, Tabernas, Spain
[f] CIESOL, Joint Centre of the University of Almeria-CIEMAT, 04120 Almeria, Spain
[g] Center of Plant, Soil Interaction and Natural Resources Biotechnology, Scientific and Technological Bioresource Nucleus (BIOREN). Universidad de la Frontera, Av. Francisco Salazar 01145, PO Box 54-D Temuco, Chile
[h] Centro de Investigación para la Sustentabilidad (CIS), Facultad de Ciencias de La Vida, Universidad Andres Bello, República 440, Santiago 8327055, Chile

ARTICLE INFO

Keywords:
Allophane nanoclays
Contaminants of Emerging Concern
Compound Parabolic Collector
Escherichia coli
Solar photocatalysis
Urban wastewater

ABSTRACT

Allophane (ALPH) nanoparticles have been traditionally employed for in-situ decontamination of soil and sediments, water and industrial effluents as well as medical therapies. In contrast, their development for water purification has not been well investigated. This study assessed for the first time the capability of several modified ALPH nanoclays as potential photocatalysts for water disinfection and decontamination. Concentrations ranged from 0 to 200 mg L^{-1} of pristine ALPH, Fe-ALPH, TiO_2-ALPH, Fe-TiO_2-ALPH, Fe-ZnO-ALPH and ZnO-ALPH were evaluated at laboratory (200 mL) and pilot plant scale (10L-Compound Parabolic Collector, CPC), in demineralized water (DW) and actual urban secondary wastewater effluents (SW) under solar radiation. The photocatalytic efficiency was evaluated through the simultaneous monitoring of the inactivation of *Escherichia coli* and the removal of imidacloprid and sulfamethoxazole (Contaminants of Emerging Concern, CECs). The best simultaneous disinfection and decontamination performance (80 % $\sum$CECs and > 5 Log Reduction Value (LRV) *E. coli*) was obtained for TiO_2-ALPH both in DW and SW at 200 mg/L; while the higher disinfection capability (> 5 LRV in 30 min or 2.5 kJ/L of Q_{UV}) was obtained with ZnO-ALPH. Both catalysts were then assessed in 10L-CPCs demonstrating the potential up-scaling of these friendly-photocatalytic materials for wastewater reclamation.

1. Introduction

The quality and availability of safe water is now one of the most serious challenges facing the planet. In this context, industrial practices and human activities play an essential role in the release of a great variety of pollutants into water bodies. One viable solution to reduce the stress on water resources is the reclamation and reuse of urban secondary wastewater effluents (SW), thus contributing to a circular economy in line with the Sustainable Development Goal 6 of the United Nations (reuse and sustainable use of urban wastewater by 2030) [1]. In this context, the organic matter and microbial load are the main concerns of the traditional treatments for wastewater reclamation. Moreover, they are not capable of eliminating the so-called Contaminants of Emerging Concern (CECs) and, for this reason, different authors have reported the presence of CECs at low levels in water bodies (ranging from ng L^{-1} to μg L^{-1}), with increased rates in recent years. The primary concern associated with the CECs is the lack of knowledge of their long-term effects on human health and the environment [2,3]. CECs include a wide range of compounds, such as pharmaceutical and personal care products, surfactants, flame retardants, gasoline additives, fertilisers, pesticides, and endocrine-disrupting compounds, among others [4–6]. Therefore, it is necessary to develop new wastewater

* Corresponding author.
E-mail address: mpolo@psa.es (M.I. Polo-López).

https://doi.org/10.1016/j.cej.2024.157894
Received 18 August 2024; Received in revised form 8 November 2024; Accepted 20 November 2024
Available online 23 November 2024
1385-8947/© 2024 Elsevier B.V. All rights are reserved, including those for text and data mining, AI training, and similar technologies.

treatments for an environmentally friendly removal of CECs and microbial pathogens from aquatic systems. In this sense, advanced oxidation processes (AOPs) are a promising alternative. AOPs are processes based on the generation of radical species able to oxidize organic matter and, by extension, inactivate pathogens in water. For that purpose, different strategies have been investigated, including solar-driven photocatalysis as a promising and sustainable alternative or complementary method for wastewater treatment [7–10].

Heterogeneous photocatalysis employs semiconductor materials as photocatalysts, whose reaction mechanism is well understood. Thus, when the photocatalyst is irradiated with energy equal to or greater than its bandgap, electrons are excited from the valence band to the conduction band, and an electron-hole (e^-/h^+) pair is generated. The photo-induced species can interact with an electron acceptor, such as O_2, and water on the surface of the particles, generating hydroxyl radicals ($HO^\bullet$) and superoxide radicals ($O_2^{\bullet-}$) [7,10].

On the other hand, in the last decades, clay minerals have garnered significant attention as a promising solid support for the incorporation or impregnation of semiconductors, leveraging their exceptional properties [11–13]. Allophane (ALPH) nanoclay has been investigated due to its cost-effectiveness, being environmentally friendly and stable structures, facilitating catalyst recycling. ALPH is characterized by its regularly arranged silica-alumina and nanospherule structures, high adsorption capacities, large specific surface areas, substantial cation exchange capacities, and surface electronegativity [14–17]. However, ALPH has been primarily investigated in the fields of medicine, soil and sediment remediation, and contaminant adsorption processes [18,19]. While their development for water purification has not been well investigated; however, due to their physicochemical characteristics, it could enhance the interaction between the active sites of the photocatalyst and both organic contaminants and microbial pathogens, thereby improving photocatalytic activity.

Recently, the capability of modified ALPH nanoclays with iron oxide and/or titanium dioxide (TiO_2), and/or zinc oxide (ZnO) for water decontamination has been slightly reported in the literature, while there are no studies dealing with its application for water disinfection. A > 99 % removal of atrazine (ATZ) together with the decrease of chemical oxygen demand (by 85 % and 35 % after 4 h at initial pH 3.0 and 5.0, respectively) has been reported by using ALPH nanoclay modified with 6 % of iron oxide and 30 % w/w of TiO_2 under natural sunlight [8]. Chemical and physical characterization of these materials revealed that the presence of iron oxide on ALPH generated a decrease in the band gap energy for different catalysts, broadening the photo-response range to visible light, and improving, therefore, the photocatalytic performance.

The main goal of this study is the assessment for the first time of different catalysts based on ALPH nanoclay modified with Fe, TiO_2 and ZnO for the simultaneous photocatalytic disinfection (*E. coli*) and CECs removal (IMD and SMX) from water. The study examined the influence of catalyst concentration and physicochemical composition of the water matrix (demineralized water (DW) and SW) on the photocatalytic performance of each developed material. A preliminary proof-of-principle in DW was carried out at a laboratory scale (200 mL-batch vessel reactor), and a further evaluation in SW and at pilot scale in a 10 L-Compound Parabolic Collector (CPC) photoreactor was performed, all under natural sunlight.

2. Materials and methods

2.1. Reagents

Imidacloprid ((E)-1-(6-chloro-3-pyridylmethyl)-N-nitroimidazolidin-2-ylideneamine, PESTANAL, analytical standard), sulfamethoxazole (4-Amino-*N*-(5-methyl-3-isoxazolyl) benzenesulfonamide, N^1-(5-Methyl-isoxazol-3-yl) sulphanilamide), SUPELCO, analytical standard), iron (III) nitrate nonahydrate ($Fe(NO_3)_3{\cdot}9H_2O$, > 98 %) and zinc nitrate hexahydrated ($Zn(NO_3)_2{\cdot}6H_2O \geq 98$ %) were purchased from Sigma-Aldrich. Sulphuric acid (H_2SO_4, 97 %), sodium hydroxide (NaOH ≥ 99 %), formic acid (HCOOH ≥ 98 %), acetonitrile (ACN) (CH_3CN) and methanol (CH_3OH) at gradient grade for liquid chromatography (LiChrosolv®) were supplied by Merck. All reagents were used as received. The water solutions were prepared with MilliQ water.

2.2. Catalysts preparation

In this study, seven photocatalysts have been evaluated, including the benchmark Aeroxide® TiO_2-P25 (Evonik), as it is a recognized reference of the photocatalytic activity in water [7,10,15] and six photocatalysts based on ALPH nanoclay have been prepared and tested: (i) pristine ALPH nanoclay (ALPH) and (ii) Fe-allophane (Fe-ALPH) with 6 % w/w iron oxide, were synthesized via coprecipitation of aluminium chloride and potassium silicate and a wet impregnation, respectively, according to a previous study [15]. (iii) TiO_2-allophane (TiO_2-ALPH) and (iv) Fe-TiO_2-allophane (Fe-TiO_2-ALPH) were synthetized using anatase phase of TiO_2 by acid hydrolysis using $TiCl_4$ and $Fe(NO_3)_3{\cdot}9H_2O$ as metal sources. These catalysts were prepared with a fixed iron content of 6 % w/w and titanium of 30 % w/w as described previously [8]. (v) Fe-ZnO-allophane (Fe-ZnO-ALPH) and (vii) ZnO-allophane (ZnO-ALPH) were prepared by basic co-precipitation method, using iron oxide (6 % w/w) as $Fe(NO_3)_3{\cdot}9H_2O$ and iron oxide as $Zn(NO_3)_2{\cdot}6H_2O$ (10 % w/w) and relevant details are shown in Content S1 (Supplementary material).

The characterization and physicochemical attributes of these catalysts are reported elsewhere [8]. Briefly, Table 1 summarized the most important characteristics of these catalysts analyzed by Scanning Electron Microscopy (SEM) SU3500 HITACHI-Japan equipment Back-scatter detector (BSE) coupled with energy-dispersive X-ray spectroscopy (EDX). The textural properties of the catalysts were determined by nitrogen adsorption–desorption isotherms at 77 K using 3-FLEX Micromeritics equipment. The specific surface area (S_{BET}) was evaluated using the Brunauer, Emmett, and Teller (BET) method and the pore size distribution was determined employing the Barrett-Joyner-Halenda (BJH) method. The total pore volume was determined based on the adsorbed quantity at p/p^0 of 0.99. The surface charge (ζ-potential) was determined using a Zetasizer Nano ZS90 (Malvern Instruments, Inc., Malvern, UK). The light absorption properties were assessed through diffuse reflectance spectra (DRS), using a Shimadzu UV–Vis-2450-Japan spectrophotometer, equipped with a diffuse reflectance accessory. The band gap energies (E_g) of the photocatalysts were estimated using the Kubelka-Munk (K-M) function and the Tauc plot [8].

2.3. Water matrices

In this study, two water matrices were used. DW was used to assess the performance of all the photocatalytic materials without the influence of any chemical (organic or inorganic) compounds. SW was obtained from the Municipal Wastewater Treatment Plant of 'El Bobar' in Almeria (Spain) and used to assess the photocatalytic performance in complex water matrices with high contents of organic and inorganic compounds as well as a heterogeneous microbial community. Several SW batches were freshly collected, characterized (Table S1), stored at 4 °C and used in less than 72 h to avoid potential modification of their characteristics.

2.4. CECs quantification

Two CECs (IMD and SMX) were monitored in both water matrices at 100 μg L^{-1} each, following the procedure already described in the literature [21]. They were selected as model CECs due to their frequent detection in SW or water bodies, such as rivers or lakes. A stock solution of 100 mg L^{-1} in DW was prepared and stored at 4 °C until use. Withdrawn experimental samples of 4.5 mL were immediately filtered (0.2 μm), the filter was also washed with 0.5 mL of ACN to remove any adsorbed organic compounds, and then analysed by Ultra Performance

Table 1
Chemical composition, structural properties, ζ potential and bandgap values (Eg) of ALPH and modified ALPH with iron, TiO_2 and ZnO.

Catalyst	Chemical composition						Structural properties			Optical properties	ζ potential at pH 7
	Ti	Zn	Fe	Si	Al	Si/Al ratio	S_{BET}	Vp	dp	Eg	mV
	wt %						$m^2\ g^{-1}$	$cm^3\ g^{-1}$	nm	eV	
ALPH	–	–	–	69.0	39.0	2.20	147	0.418	10.6	n.d	−43 ± 1.3
Fe-ALPH	–	–	14.4	60.9	24.8	2.90	135	0.520	14.5	1.71	−44 ± 1.6
ZnO-ALPH	–	8.90	–	29.9	11.2	2.68	51.3	0.361	28.1	3.04	−49 ± 2.4
Fe-ZnO-ALPH	–	11.90	4.86	36.4	13.9	2.63	117	0.527	18.1	2.27	−45 ± 2.7
TiO_2-ALPH	23.8	–	–	19.8	3.9	5.08	577	0.925	6.41	3.24	−36 ± 0.5
Fe-TiO_2-ALPH	20.1	–	4.20	17.1	3.4	5.03	227	0.360	6.40	2.35	−10 ± 0.8
TiO_2-P25*	≥99.5	<0.01	<0.01	<0.2	<0.3	–	50 ± 15	0.310	30.0	3.00	−10 ± 1.5

* Data from the manufacturer [20].

Liquid Chromatography (UPLC). The CECs concentration was monitored by UPLC/UV Agilent Technologies (USA, Series 1200 equipment) provided with a diode array detector and a C-18 analytical column (Poroshell 120, EC-C18 3.0 mm x 50 mm, 2.7 μm particle size), according to Berruti et al., 2022 [21]. Briefly, 100 μL of samples was injected under a flow rate of 1 mL min^{-1} with 95 % 25 mM formic and 5 % ACN as the initial condition. A linear gradient progressed from 5 % ACN to 90 % in 12 min and then at 100 % for 1 min. The re-equilibration time was 3 min. SMX and IMD were detected at 267 and 273 nm and at different retention times, 5.1 and 4.5 min, respectively. The quantification limit for both pollutants was 5 μg L^{-1}. This quantification procedure was carried out similarly in both types of water matrices. The treatment efficiency for contaminants removal was established at 80 % removal, according to the Swiss SW regulation [22].

2.5. Escherichia coli enumeration and quantification

The culture-type *E. coli* K-12 was evaluated in DW. This bacterium strain was provided by the Spanish Culture Collection (CECT, reference 4624) and it was grown in Luria-Bertani Broth (Merck KGaA®, Darmstadt, Germany). A suspension with a concentration of ~ 10^9 Colony Forming Units (CFU) mL^{-1} was obtained after 20 h of incubation (37 °C and 100 rpm in a rotary shaking incubator) and centrifugation for 15 min at 3000 rpm. Bacterial pellets were re-suspended in phosphate-buffered saline solution (Sigma-Aldrich®, USA) and directly diluted in the water to obtain an initial concentration of 10^6 CFU mL^{-1}. Dissolved Organic Carbon (DOC) of spiked DW was measured and data is included in Table S1. DOC concentration of 1.6 mg L^{-1} was detected, discarding, therefore, any significant effect on the photocatalytic efficiency in this water matrix.

Bacterium concentration was monitored through the standard plate counting method. Samples were dropped (3x20 μL of 10x diluted samples) or, for lower expected concentration, 500 μL of non-diluted samples were spread on Petri dishes containing ENDO Agar (Merck KGaA®, Darmstadt, Germany) and incubated for 48 h at 37 °C. Detection limit (DL) was 2 CFU mL^{-1} [21,23,24].

In the case of SW samples, the naturally occurring *E. coli* was monitored through the standard plate counting method. In brief, 50 μL and 500 μL of non-diluted water samples were spread on Petri dishes with ChromoCult® Coliform Agar (Merck KGaA, Darmstadt, Germany), and incubated for 24 h at 37 °C. DL was 2 CFU mL^{-1} [21].

2.6. Photoreactors

Lab-scale tests were carried out using 250 mL batch vessels (DURAN Glass, Schott, Germany) as photoreactors, described elsewhere [25]. They are made of borosilicate glass and covered with a glass lid (Schott®) to allow solar radiation to enter from all directions and equipped with a magnetic stirrer. Each vessel had the following characteristics: 90 % UVA-transmission of borosilicate (cut-off at 280 nm), 200 mL of total and irradiated volume, 0.15 m of total length, 0.05 m of external diameter, 0.002 m of wall thickness and 0.0095 m^2 of irradiated surface.

Pilot-scale tests were carried out using a 10L-CPC photoreactor, described in detail elsewhere [25]. Briefly, the CPC photoreactor is comprised of one module consisting of a Pyrex glass tube surrounded by a mirror made of anodized aluminium (MiroSun®), and mounted on a south-facing platform tilted at the same angle as the local latitude (37°). The total volume of water is 10 L, the illuminated volume is 2.5 L, and 0.075 m^2 of illuminated collector surface. The water flows from a recirculation tank (10 L) to the photoreactor tubes by a centrifugal pump (turbulent flow rate of 25 L min^{-1}). Two identical modules of CPC were used in this study, allowing to perform simultaneously two duplicates of the same operational condition.

2.7. Experimental procedure

All tests were carried out at Plataforma Solar de Almeria (Almeria, Spain, latitude: 37.0909°N, longitude: 2.357°W) in outdoor conditions. CECs stock solution and *E. coli* stock suspension were directly and simultaneously diluted in the solar vessels previously filled with DW to achieve the desired initial concentrations (100 μg L^{-1} of each contaminant and 10^6 CFU mL^{-1} for *E. coli*), subsequently, the required amount of catalyst was added to reach concentrations ranging from 0 to 200 mg L^{-1}. In the case of SW, the procedure was similar, except for bacteria, as the naturally occurring *E. coli* was monitored. The suspension was homogenized under dark conditions in both photoreactors, and a sample was taken as a control of the initial concentrations. After that, photoreactors were exposed to natural sunlight and samples for quantification of CECs and *E. coli* were taken out at specific time intervals. All experiments were performed at the initial naturally occurring water pH. Turbidity (turbidimeter model 2100AN, Hach, USA), water temperature (portable thermometer model CRISON TM 65, CRISON INSTRUMENTS S.A., Spain), and pH (portable pHmeter LAQUAact-pH110, Horiba, Japan) were monitored at the beginning and the end of the experimental time (Table S2-S3). Water temperature never exceeds 40 °C, discarding any significant thermal effect in bacteria inactivation nor photocatalyst activity [21]. Water pH ranged, for all catalysts, at circumneutral pH (6.8), remaining almost constant during the treatment time and discarding this parameter as a key role in the mere disinfection or degradation of CECs. Dissolved organic carbon (DOC) was also monitored by using a Total Organic Carbon analyzer (Model TOC-L, Shimadzu, Japan), and no differences were observed between the initial and final values obtained, ranging from 1.8 and 2.3 mg L^{-1} for DW, and from 19.6 to 23.9 mg L^{-1} for SW, discarding this parameter as a key factor to assess the efficiency of the investigated photocatalysts.

All experiments, starting at 11:00 a.m. local time, were performed for 4 h on completely sunny days, with duplicate runs. The incident solar radiation was monitored using a pyranometer (Kipp & Zonen, CUV5, Netherlands), which measured the solar UV-A irradiance (range 280–400 nm) in W m^{-2}. The minimum and maximum values obtained during the experiments were 25.2 ± 6.1 and 36.7 ± 5.4 W m^{-2},

respectively. The irradiance data were also used to calculate the Q_{UV} parameter (the accumulative energy per unit of volume, kJ L^{-1}) using Eq. (1) for each experiment, thus allowing the comparison under different irradiances, photoreactors and experimental conditions [26].

$$Q_{UV}\left(\frac{kJ}{L}\right) = \frac{\sum_n UV_{n-1}\left(\frac{W}{m^2}\right)A_r(m^2)}{V_t(L)}\frac{\Delta t(s)}{1000} \quad (1)$$

where Q_{UV} is the UV energy accumulated per litre (kJ L^{-1}) at time n; UV_{n-1} is the average incident radiation on the irradiated area; A_r is the irradiated area (m^2); Δt is the experimental time of the sample; and V_t is the total volume (L).

2.8. Kinetic analysis

The degradation of contaminants and the inactivation of bacteria followed pseudo-first-order kinetics, and they were calculated according to Equations Eq. (2) and Eq. (3).

$$\frac{dC}{dt} = -kC \quad (2)$$

$$ln\frac{C_t}{C_0} = -kQ_{UV} \quad (3)$$

where C_0 and C_t represent the CEC or *E. coli* concentration at the time 0 and at certain Q_{UV} (kJ L^{-1}), respectively. k, the pseudo-first-order kinetics constant (L kJ^{-1}) can be evaluated from the slope of the natural logarithm of the change in concentration of CECs or *E. coli* against the Q_{UV} plot if a right line is obtained.

3. Results and discussion

3.1. Dark assessment

The viability of *E. coli* and the adsorption of each CEC (IMD and SMX) in the presence of 200 mg L^{-1} of each photocatalyst were tested in the dark during 3 h of contact time (Fig. 1). In the case of CECs, it was observed that there is no significant effect of the catalysts on adsorption processes. Within the first hour of contact, there is a small decrease, between 5 % and 10 %, followed by a stationary phase where no differences are observed. These results are consistent with previous studies with ALPH modified with TiO_2, ZnO, Fe, and Cu, finding adsorption between 5 % and 15 % of atrazine and phenol (10 mg L^{-1}) at different initial pH values after 30 min of contact time [8,15–17]. This effect can be attributed to the mesoporous characteristic of the materials, with a high S_{BET}, and pore diameter (dp, nm) (Table 1), which favours interaction between contaminants and catalysts [8].

Regarding *E. coli,* in the presence of ALPH, Fe-ALPH, TiO_2-ALPH, and Fe-TiO_2-ALPH, the concentration showed a slight decrease over 3 h (< 0.5 Log Reduction Values, LRV). However, no significant reduction was observed, demonstrating no toxic effect on the bacterial viability, neither due to the presence of the catalysts nor the CECs at the concentration added. Therefore, the effect observed under natural sunlight in the presence of the photocatalysts is likely due to photocatalysis.

Otherwise, the catalysts based on ZnO (ZnO-ALPH and Fe-ZnO-ALPH) exhibited a decrease of 2 LRV in *E. coli* after 3 h of contact time. This result is consistent with findings reported by various researchers, where ZnO nanoparticles demonstrated antibacterial activity under dark conditions [27–29]. This antibacterial activity is mainly attributed to: (i) morphological effect due to the physical rupture of cell membranes or deformation, (ii) cell toxicity by the dissolution of Zn^{2+} ions, and (iii) Reactive Oxygen Species (ROS) generation by ZnO particles due to the potential oxygen defect sites (surface defects of oxygen vacancies Vo^0, Vo^+, Vo^{2+} (0.05–3.1 eV) of the nanoparticles, which may act as electron donors to the conduction band of ZnO [27–30]. In Fig. 1,

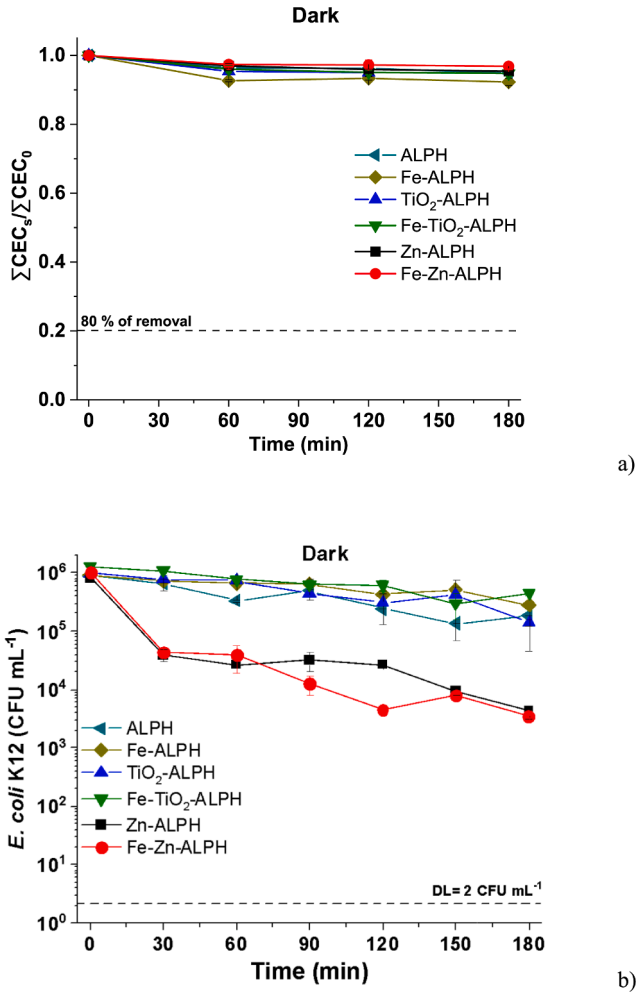


Fig. 1. Degradation of CECs (a) and inactivation of *E. coli* (b) using different catalysts at a concentration of 200 mg L^{-1} under dark conditions.

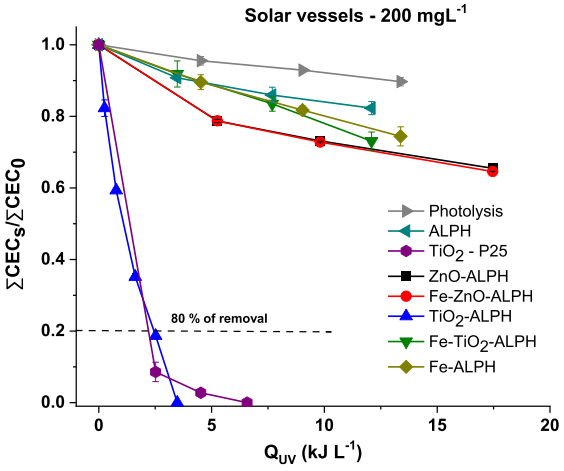
similar inactivation profiles are observed for ZnO-ALPH and Fe-ZnO-ALPH catalysts, where initially, there was a rapid decrease (1.5 LRV in the first 30 min) followed by a slower decay (0.5 LRV in 2.5 h). This could be attributed to the initial dissolution of Zn^{2+} ions, along with the direct contact effect of ZnO-ALPH nanoparticles with cell walls, affecting bacterial cell integrity that eventually ends in cell death. The solubilization of Zn^{2+} has been quantified through atomic absorption, under these operating conditions (200 mg L^{-1} and dark condition), finding 0.905 mg L^{-1} and 0.882 mg L^{-1} of Zn^{2+} for ZnO-ALPH and Fe-ZnO-ALPH, respectively. The low antibacterial activity aligns with findings reported by Núñez-Salas [31], where a decrease of 1.5 LVR of *E. coli* was reported using ZnO nanoparticles in distilled water in 1.5 h of contact time. In addition, the detected Zn^{2+} concentrations are below the maximum permissible (5 mg L^{-1}) guidelines for potable and surface water [32,33], discarding the measured concentration in this study as a source of toxicity for humans or the environment.

Therefore, for ALPH, Fe-ALPH, TiO_2-ALPH, and Fe-TiO_2-ALPH catalysts, the target removal kinetics can be attributed mainly to the photocatalytic activity (generation of ROS) rather than effects of the Fe, TiO_2 and/or ALPH on both bacterium viability or CECs adsorption. In the case of ALPH-based ZnO, despite the slight effect on *E. coli* in the dark, it is expected that the greatest effect on bacterial inactivation and degradation of CECs will occur through solar photons, Zn^{2+} effects and/or by the generation of ROS resulting from the photocatalytic activity under natural sunlight.

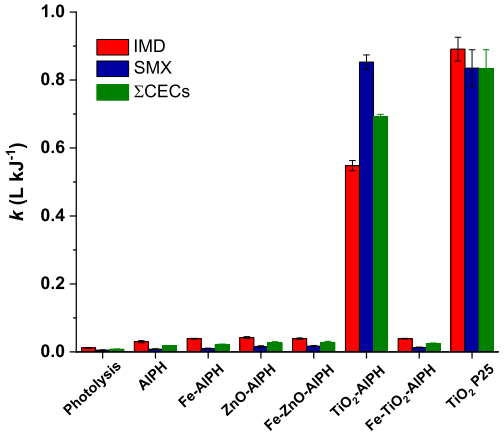
3.2. Solar-only radiation assessment

It is well-known that the mere effect of solar UV and visible photons may play a role in the degradation of organic compounds and microorganisms in water, therefore, the direct photolysis of CECs and the inactivation of *E. coli* were assessed before photocatalysis to determine its impact over the targets under evaluation (Fig. 2). For CECs, a small contribution from photolysis can be observed after 3 h of solar exposure, with a 5–10 % decrease in SMX and IMD concentrations, and similar findings have been reported in previous studies [21].

The effect of natural solar radiation on *E. coli* viability showed a total inactivation (DL = 2 CFU mL^{-1}) after 120 min of solar exposure (9.0 kJ L^{-1} of Q_{UV}) (Fig. 3). A kinetic constant of 0.689 ± 0.039 L kJ^{-1} was calculated (Table S4), which agrees with data reported in other works reporting solar inactivation of *E. coli* K-12 under similar operational conditions [23]. The inactivation phenomenon is primarily ascribed to the synergistic effect of solar UV photons and water temperature [34,35]. It is widely acknowledged that the absorption of solar photons can induce the generation of intracellular ROS, including $O_2^{\bullet}$, $HO^{\bullet}$, and $HO_2^{\bullet}$, which are capable of damaging DNA, proteins, lipids, and enzymes, leading to the accumulation of cellular damage and eventually to the cell death. It is noteworthy that temperature, a key factor in microbial inactivation, was monitored in all experiments. It was below 32 °C, being, therefore, dismissed in this study as a pivotal factor in bacterial inactivation [34].

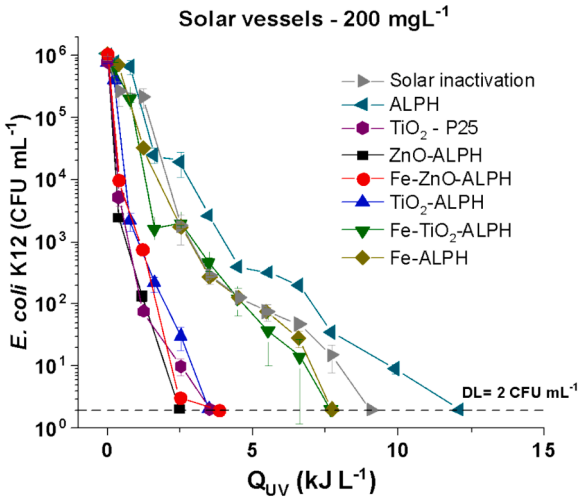


a)

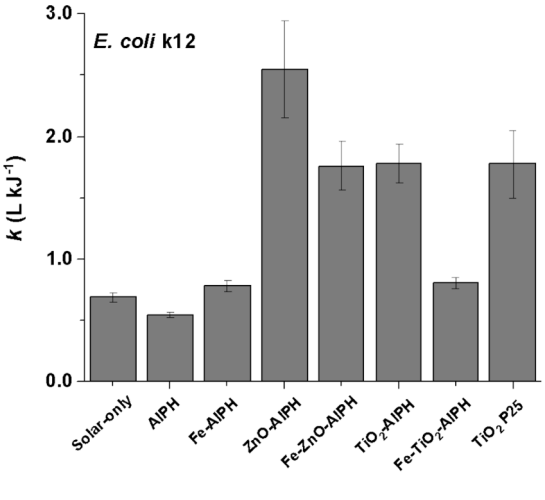


b)

Fig. 2. (a) Degradation of CECs and (b) associated kinetics constants obtained in DW by all photocatalysts at a concentration of 200 mg L^{-1} under natural sunlight and in vessel reactors.



a)



b)

Fig. 3. (a) Inactivation profiles of *E. coli* and (b) associated kinetics constants obtained in DW by all photocatalysts at a concentration of 200 mg L^{-1} under natural sunlight and in vessel reactors.

3.3. Photocatalytic performance in demineralized water

The photocatalytic capability of pristine ALPH, modified-ALPH photocatalysts and Aeroxide TiO_2-P25 as a reference was simultaneously investigated against CECs removal and *E. coli* inactivation under natural solar radiation. A concentration of 200 mg L^{-1} was selected for comparison of the disinfection and decontamination photocatalytic performance of all materials, according to previous works [21]. In general, the addition of the investigated photocatalysts caused different effects depending on the type of modified ALPH and the type of target (CECs or bacteria).

3.3.1. Photocatalytic removal of CECs

Fig. 2 and Table S4 show the profiles of degradation of ∑CECs and kinetics parameters, respectively, obtained by all the photocatalysts investigated at 200 mg L^{-1}. The degradation profiles of IMD and SMX are depicted in Figure S1. Results showed that ALPH and modified-ALPH nanoclays did not exhibit successful degradation efficiencies, except for TiO_2-ALPH, which reached similar results to TiO_2-P25. At the concentration tested, the following order of reactivity was found: Photolysis (no catalysts) (10 %) < ALPH (17 %) < Fe-ALPH (25 %) ≈ Fe-TiO_2-ALPH (26 %) < ZnO-ALPH (35 %) ≈ Fe-ZnO-ALPH (35 %) < TiO_2-ALPH (99 %) ≈ TiO_2-P25 (99 %). The best performance was reached by TiO_2-

ALPH, demonstrating heightened catalytic efficacy in CEC degradation compared to all catalysts, resembling TiO_2-P25. This catalyst achieved the Swiss regulation limit of > 80 % degradation of CECs in 45 min of solar radiation (3.1 kJ L^{-1} of Q_{UV}) (Fig. 2).

On the other hand, it can be also noted that IMD showed a slightly higher reactivity (20–29 %) in comparison with SMX (Fig. 2b) for all the photocatalysts, except for TiO_2-ALPH where the faster degradation did not permit observing this behaviour. The reactivity difference can be attributed to the zeta potential (surface charge) of each nanoparticle at the working water pH 7–8 (Table 1) and the contaminants. At this condition, all nanoparticles (ALPH and modified-ALPH) and SMX show a negative surface charge, which may generate an electrostatic repulsion between the catalysts and the SMX, resulting in a lower interaction and a lower oxidation rate compared to IMD. In addition, IMD has a net negative charge, but it has an imidazolidine ring and a C=N bond coupled NO_2, which is a strong electron-withdrawing group, therefore, the bond has a small positive charge [36] and it may help to explain the slightly higher reactivity.

3.3.2. Photocatalytic inactivation of E. coli

Fig. 3 shows the inactivation profiles and kinetics constants of *E. coli* with all ALPH nanoclays, in comparison with solar-only radiation and TiO_2-P25 as reference. The detection limit (2 CFU mL^{-1}) from an initial concentration of 10^6 CFU mL^{-1} was obtained in all cases, yielding > 5 LRV under natural sunlight. All the catalysts enhanced the disinfection kinetics of the mere effect of solar-only radiation (no catalysts), except ALPH nanoclay. Best *E. coli* inactivation performance was obtained with ZnO-ALPH and Fe-ZnO-ALPH, reaching DL in 30–45 min of treatment time (2.5–3.8 kJL^{-1} of Q_{UV}). Table S4 shows the associated kinetics constants, where ZnO-ALPH shows an increase of the *k* of 1.4 times compared to Fe-ZnO-ALPH, TiO_2-ALPH and TiO_2-P25 catalysts, and 3.7 times in comparison to solar-only radiation (*k* of 2.55, 1.76, 1.78, 1.78 and 0.69 L kJ^{-1}, respectively). The following order of *E. coli* inactivation was observed: ZnO-ALPH > Fe-ZnO-ALPH ≈ TiO_2-P25 ≈ TiO_2-ALPH > Fe-TiO_2-ALPH > Fe-ALPH > ALPH.

Therefore, modified-ALPH nanoclays with ZnO showed, under these experimental conditions, great antibacterial potential, but in comparison with CECs removal, this catalyst did not show an efficient photocatalytic performance. Successful disinfection and decontamination trend was only observed for TiO_2-ALPH and TiO_2-P25, where both inactivation of *E. coli* and > 80 % degradation of CECs, were achieved after 45 min of solar treatment time (3.5 kJ L^{-1} of Q_{UV}) (Table S4 and Fig. 2).

3.3.3. Proposed photocatalytic decontamination and disinfection mechanisms

The results obtained for both CECs removal and *E. coli* inactivation have demonstrated different trends in terms of catalyst efficiency. This

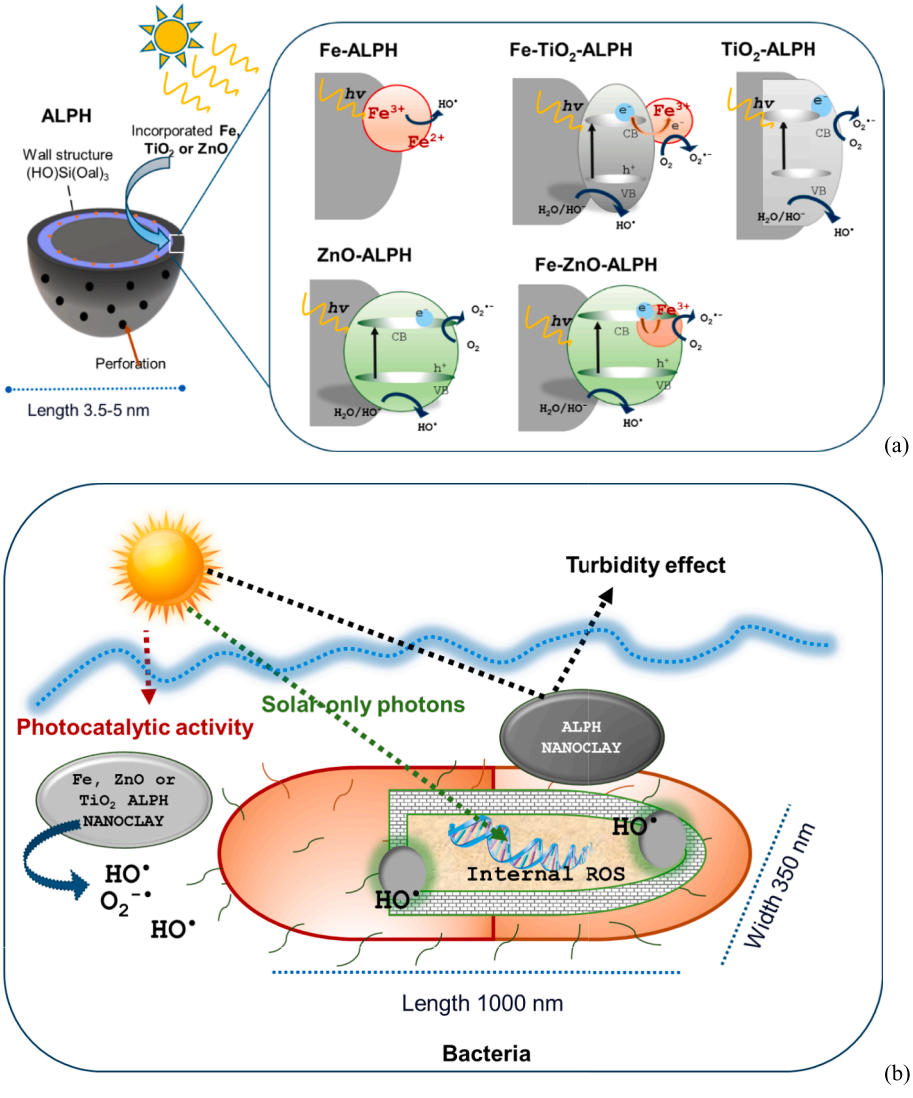


Fig. 4. (a) Schematic representation of the different catalysts investigated and (b) proposed bacterial inactivation mechanisms.

difference can be attributed to the different photocatalytic activity (ROS generation) (Fig. 4a) and the mechanisms associated specifically with the interaction with CECs and bacteria (Fig. 4b). In addition, to discard modifications of the trend results as a consequence of a potential competition for ROS produced between the bacteria and contaminants, degradation of CECs was conducted under the same experimental conditions, but without the presence of *E. coli* (Figure S2). A slight increase in CECs degradation (< 7 %) was observed for all nanoclays without the presence of bacteria in comparison with their presence. This result stated that there is no significant competition or influence on the trend results obtained during the photocatalytic processes due to the simultaneous CECs degradation and *E. coli* inactivation.

Therefore, after being discarded thermal effects, chemicals (such as DOC content) influence, competition between biological and CECs targets and pH fluctuations on the results, the different behaviour obtained by the modified-ALPH catalysts can be attributed to the following potential mechanisms:

(i) ALPH nanoclay is an aluminosilicate that does not absorb light, and, therefore, it has no photocatalytic activity [8], consequently, and as expected, the lowest efficiency in comparison with the other photocatalysts was observed. Regarding CECs removal, a smooth enhancement in comparison with photolysis was obtained, which can be due to the adsorption–desorption behaviour, also observed in dark conditions and attributed to its morphological characteristic (mesoporous material with a high S_{BET})[15,17,37,38,8]. For *E. coli*, the addition of ALPH nanoclays determined lower kinetics in comparison with solar-only disinfection (no catalyst). This behaviour is attributed, in addition to the absence of photocatalytic activity, to the turbidity generated by the presence of suspended ALPH nanoclay (77 NTU) (Table S2). It is well documented that turbidity hinders the penetration of solar photons into the solution, which may reduce the bacterial inactivation rate compared to the solar-only process [34,35]. At these conditions, the absorption of solar photons by cell components, required for the effective inactivation of bacteria as previously described by solar-only disinfection, is limited. As a consequence, the generation of potential intracellular ROS is lower in comparison with solar-only inactivation, and simultaneously, the suspended particles act as a protection screen for bacteria (Fig. 4b), leading to lower microbial inactivation kinetics.

(ii) Fe-ALPH, in which incorporation of iron contents could be expected to exhibit photocatalytic properties [15,16,39,8]. Nevertheless, under our experimental conditions, this catalyst exhibited for both CECs degradation and *E. coli* inactivation a similar efficiency compared with ALPH nanoclay. In literature, the influence of initial pH on the removal of pollutants using iron oxides by photocatalytic process has been reported, concluding that acidic pHs are more beneficial than alkaline pHs [40,41]. This can explain why the catalytic efficiency obtained in our results, performed at neutral pH, is lower in comparison with the other catalysts. On the other hand, at this concentration (200 mg L^{-1}), iron species (Fe(II) or Fe(III)) in solution were not detected, either in darkness or under solar light, at our working pH, discarding any homogenous photocatalytic effect in the results.

(iii) ZnO-ALPH exhibits higher CECs degradation compared to ALPH and Fe-ALPH, but still poor efficiency. The results may be due to several factors, being the pH of the solution the most important and responsible for the low CECs degradation kinetics obtained herein at neutral pH (Table S1). Previous studies have reported an enhanced catalytic activity of Fe-ZnO and Fe-TiO_2-ALPH at initial acidic pH, with an efficiency decrease as the pH increase and reaching the best results between an initial pH of 3 to 5, a similar effect has been reported for Fe-ZnO and ZnO nanocomposites [42,43].

In the case of bacterial inactivation kinetics by ZnO-based catalysts, a synergism is evidenced between the previously described toxic effect of Zn^{2+} in the dark, coupled with the production of ROS through the photocatalytic process (Reaction R(1) to R(4)), which in this case explain the fast kinetics obtained, even at neutral pH.

$$Catalyst + h\nu \rightarrow e^- + h^+ \quad \text{(R1)}$$

$$h^+ + H_2O \rightarrow H^+ + OH \quad \text{(R2)}$$

$$e^- + O_2 \rightarrow O_2^-\cdot \quad \text{(R3)}$$

$$e^- + O_2 + H^+ \rightarrow HO_2 \quad \text{(R4)}$$

Regarding catalysts based on ZnO, Zn^{2+} concentrations of 0.76 mg L^{-1} and 0.65 mg L^{-1} for ZnO-ALPH and Fe-ZnO-ALPH were detected, respectively, indicating a small amount of Zn^{2+} into the solution. These results suggest that while there may be a minor contribution from leached Zn^{2+} to the photocatalytic process, the concentration detected is almost negligible, and it can be assumed that the reaction primarily occurs in the heterogeneous phase, with the main contribution to degradation coming from the solid catalyst.

(iv) TiO_2-ALPH demonstrated heightened catalytic efficacy in CECs degradation compared to all catalysts, resembling TiO_2-P25. Although the kinetic constants for CECs degradation were approximately one-third lower compared to TiO_2-P25, this is primarily due to the latter's significantly higher initial velocity (Table S4 and Fig. 2a). The results obtained may be due to the higher specific surface area exhibited by this catalyst, compared to the parental and the other modified ALPH clays (577 m^2 g^{-1}, Table 1). In addition, another significant factor is the crystalline structure of TiO_2 supported on ALPH, which is found in the anatase structure, as reported in previous work [8]. Anatase structure has been widely reported as the best photocatalyst, exhibiting high activity in the generation of ROS and high efficiency in degradation pollutants [44–46]. Accordingly, the dispersion of TiO_2 on the ALPH nanoclay enhances its photocatalytic activity and it can form small particles of TiO_2 anatase on the ALPH surface (Fig. 4a), which provides more active sites for the photocatalytic degradation of CECs. This phenomenon is favoured by the reduction of particle agglomeration facilitated by the presence of ALPH clays, an effect that has been described in previous works for other clays modified with TiO_2 [8,14,44,47].

(v) Fe-TiO_2-ALPH and Fe-ZnO-ALPH: the strategy of incorporating Fe on the structure of both modified ALPH with TiO_2 and ZnO was expected to increase the photocatalytic water treatment capacity. Nevertheless, results showed lower or similar removal kinetics (for both CECs degradation and *E. coli* inactivation) as observed with TiO_2-ALPH and ZnO-ALPH. These results could be explained considering the amount of iron-loaded on the ZnO-ALPH and TiO_2-ALPH catalysts (6 % w/w of Fe, 10 % w/w Zn and 30 % w/w TiO_2) and it may not be fully incorporated into the crystal lattice, with precipitation of the excess on the surface of the ALPH clays, forming small particles of iron oxide [16]. As a consequence, Fe^{3+} acts as a recombination center, reacting with electrons and generating Fe^{2+} ($Fe^{3+} + e^- \rightarrow Fe^{2+}$), which then reacts with the hole and regenerates Fe^{3+} ($Fe^{2+} + h^+ \rightarrow Fe^{3+}$) [48–50]. Therefore, these factors can decrease photocatalytic activity, as it has been observed in the obtained results.

3.4. Effect of catalyst concentration on photocatalytic activity

One of the most important parameters in photocatalysis for the optimization of the process is the catalyst concentration since it can influence both photoactivity, owing to its intensive adsorption property, and on its ability to generate $HO^{\bullet}$ [51,52]. Therefore, different catalyst concentrations (25, 50, 100 and 200 mg L^{-1}), selected based on previous studies performed in similar solar reactors for water purification [21], were evaluated for simultaneous CECs removal and *E. coli* inactivation under solar radiation. Fig. 5a and b show the *k* constants for CECs and *E. coli*, respectively, and corresponding data are summarized in Table S4. The degradation profiles of IMD and SMX and the inactivation of *E. coli* are shown in Figures S3, S4 and S5, respectively. In addition, turbidity generated by the different loads of catalysts could play a key role in the pollutants' removal kinetics from water. Figure S6 shows the linear

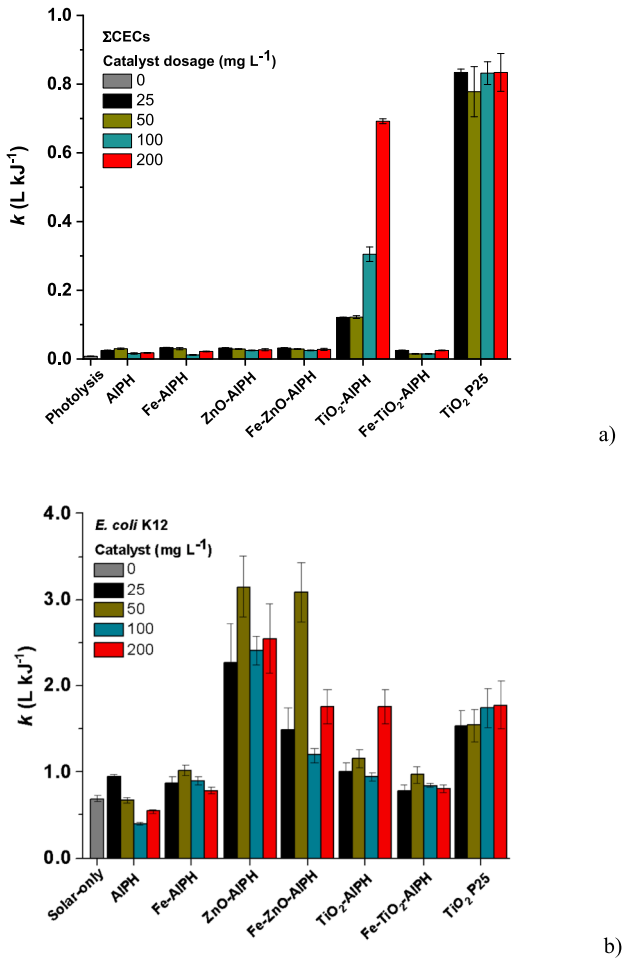


Fig. 5. Kinetics constants of (a) CECs degradation and (b) *E. coli* inactivation by all photocatalysts at different concentrations in DW under natural sunlight.

relation obtained for all catalysts at each concentration tested with their respective turbidity value obtained. In general, the higher the concentration of catalyst, the higher the water turbidity.

Regarding ALPH nanoclay and Fe-based ALPH catalysts (Fe-ALPH, Fe-TiO_2-ALPH and Fe-ZnO-ALPH), kinetics trend for both CECs degradation and *E. coli* inactivation were similar, i.e., the lower the catalyst concentration, the higher the kinetic rate from 200 mg L^{-1} to 25 mg L^{-1}. A linear trend is observed between catalytic efficiency and turbidity, revealing a decrease of 2 times in degradation percentage values for a concentration of 200 mg L^{-1} in comparison with 50 mg L^{-1}, resulting in a reduction in k_1 between 1.5 and 2 times (Table S4). This behaviour could be explained by considering the lower photocatalytic efficiency of these materials and the increased water turbidity with the catalyst load (Table S2, Figure S6). Lower catalyst concentration (50 mg L^{-1}), less amount of particles in suspension, which favours the penetration of photons into the inner layers of the catalyst, and in addition, for water disinfection, favours the photon absorption by the microorganisms and reduce the potential screening effect of suspended particles in comparison with higher catalyst concentration (200 mg L^{-1}), Nevertheless, in any case, kinetics reached similar values to TiO_2-P25, TiO_2-ALPH and ZnO-ALPH.

On the other hand, the photocatalytic activity of TiO_2-ALPH (Fig. 5) increased as the catalyst concentration increased for both CECs removal and *E. coli* inactivation. This result can be because a high concentration of TiO_2-ALPH particles increases the number of active photocatalytic sites, due to a high S_{BET} of the TiO_2-ALPH catalyst, resulting in an increased degradation rate. This effect has been previously reported for TiO_2 clays-supported [53–57]. Nevertheless, at the same concentration of catalysts, photocatalysis was faster for TiO_2-P25 in comparison with TiO_2-ALPH, attributed to the lower percentage of TiO_2 load present in TiO_2-ALPH catalysts (30 % of TiO_2, Table 1) in comparison with TiO_2-P25. However, it should be noteworthy a significant difference between both catalysts in terms of water turbidity (Figure S6), in line with further post-treatment catalysts removal and recovery. In fact, this values clearly demonstrate that best advantage of TiO_2-ALPH on TiO_2-P25 is that catalysts generate a lower turbidity, being easily recovered from the reaction medium. Besides, the lower amount of TiO_2, with almost no release to the water, in the case of TiO_2-ALPH can be also correlated with a lower potential environmental risks because of their higher size and, as natural clay, it is non-toxic for water or soil [52,58,59].

In the case of ZnO-ALPH, no significant difference in kinetic constants between the minimum and maximum catalyst concentrations (25 mg L^{-1} and 200 mg L^{-1}) was observed for CECs degradation, being in all cases a very low kinetic removal rates in comparison with TiO_2-based catalysts. Nevertheless, for *E. coli* inactivation, significant kinetic rates were observed for all concentrations, but a no linear correlation between k constants and catalyst concentration was obtained. The best concentration was 50 mg L^{-1}, with Q_{UV} values ranging between 2.0 and 3.0 kJ L^{-1}. The presence of ZnO with a wurtzite crystalline structure [28,29] showed significant antibacterial activity at any catalyst concentration. Additionally, a very low concentration of Zn^{2+} in solution was found, which decreased as the catalyst concentration in solution decreased (0.9 mg L^{-1}, 0.7 mg L^{-1}, 0.6 mg L^{-1}, and 0.4 mg L^{-1} in decreasing order of catalyst concentration, respectively). This indicates that the major effect occurs by the photocatalytic process. Summarizing and considering the need for the simultaneous disinfection and decontamination of water, it can be concluded that the most promising photocatalysts from the developed ALPH materials is TiO_2-ALPH (at 200 mg L^{-1}); while if only disinfection is considered, ZnO-ALPH (at 50 mg L^{-1}) showed the best performance, and discarding the others modified ALPH materials for further testing in more complex water matrices.

3.5. Photocatalytic performance in actual urban wastewater (SW)

To assess the photocatalytic performance of the developed photocatalytic materials, TiO_2-ALPH and ZnO-ALPH at 200 mg L^{-1} were selected for actual secondary effluent purification. The capability of these materials was investigated at a lab scale using the same solar vessel reactors and at a pilot plant scale using a 10L-CPC photoreactor to determine the up-scale of the photocatalytic processes. For all catalysts, the DOC concentration remained constant during the treatment time (between 18 and 20 mg L^{-1}).

3.5.1. Lab scale assessment (200 mL vessels photoreactors)

Fig. 6 and Table S5 show the photocatalytic CECs degradation and *E. coli* inactivation in SW and natural sunlight. Figure S7 shows IMD and SMX degradation profiles. Results showed that ZnO-ALPH and TiO_2-ALPH catalysts exhibited similar CECs degradation (52 and 57 %, respectively) and TiO_2-P25 achieved 79 % after 3 h of treatment time (17.9 kJ L^{-1} for ZnO-ALPH and TiO_2-ALPH, and 19.9 kJ L^{-1} for TiO_2-P25). In the case of TiO_2-ALPH and TiO_2-P25, the performances for CECs removal obtained in SW were 43 % and 20 % lower, respectively, compared with those obtained in DW. In addition, SW kinetic rates (k_{VES}, Table S5) were between 10 and 13 times lower compared to DW (k_{VES}/k_{DW}). These results are mainly due to the more complex physicochemical and microbial scenario of SW, with the presence of a higher organic (DOC = 21.9 ± 2.0 mg L^{-1}) and inorganic content (including anions such as chloride = 458.2 ± 32.1 mg L^{-1}), high turbidity and heterogeneous microbial populations and chemical species, which compete in the capture of $HO^{\bullet}$ or holes from the photocatalysts, ending in lower reaction rates [21,60]. In the case of ZnO-ALPH catalyst, the CECs degradation is not affected by the type of water matrix in comparison with TiO_2-ALPH, this effect may be attributed to the high

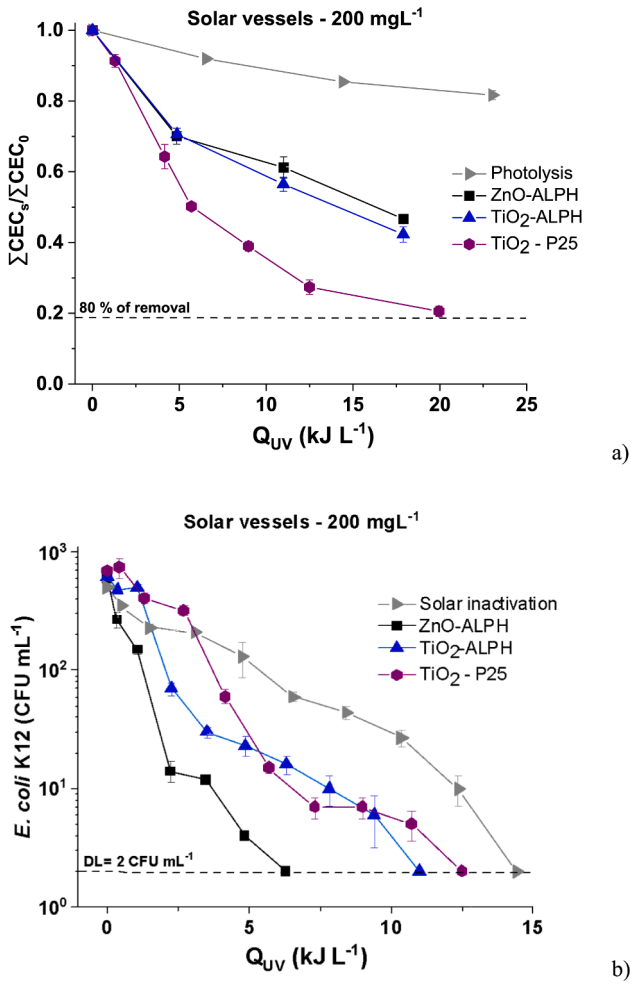


Fig. 6. Degradation of CECs (a) and inactivation of *E. coli* (b) in SW by different catalysts at 200 mg L^{-1} in vessel photoreactors and under solar radiation.

specific surface area of TiO_2-ALPH compared to ZnO-ALPH (between 10 time higher, Table 1), and a possible higher affinity of TiO_2-ALPH towards organic matter present in SW. Thus, the competition for the active sites between targets and organic matter is higher in the TiO_2-ALPH surface, compared to ZnO-ALPH. The same effect has been observed using ZnO-Ce composites, compared with TiO_2-P25 [21]. However, further investigation is necessary to obtain experimental evidence on this matter.

In the case of bacterial inactivation, Fig. 6b and Table S5 show the profiles of naturally occurring *E. coli* inactivation and associated kinetic constants, respectively. A complete *E. coli* inactivation was reached by all catalysts, following a similar reaction trend as in DW: ZnO-ALPH (6.2 kJ L^{-1} of Q_{UV}) > TiO_2-ALPH (10.9 kJ L^{-1} of Q_{UV}) > TiO_2 −P25 (12.5 kJ L^{-1} of Q_{UV}) > Solar inactivation (no catalysts) (14.9 kJ L^{-1} of Q_{UV}). ZnO-ALPH showed faster photocatalytic antibacterial activity in SW (as it was found in DW), with kinetic constant 3 times higher than TiO_2-ALPH and TiO_2-P25 (0.668, 0.239 and 0.221 L kJ^{-1}, respectively). This result confirms that ZnO-ALPH is the best catalyst for *E. coli* inactivation, in both DW and SW. Similar results have been reported by Núñez-Salas *et al.,* [31], for *E. coli* inactivation by ZnO nanocomposites, reaching complete inactivation in 60 min using simulated solar radiation and simulated SW. Berruti *et al.,* [21] reported > 5 LVR of *E. coli* in SW by ZnO-Ce catalyst after 120 min of solar exposure and 500 mg L^{-1} of catalyst concentration. On the other hand, TiO_2-ALPH showed a similar photocatalytic antibacterial action than TiO_2-P25, achieving total *E. coli* inactivation at 105 and 120 min, respectively (10.9 and 12.5 kJ L^{-1} of Q_{UV}, respectively).

3.5.2. Pilot scale assessment (CPC photoreactor)

Fig. 7 shows the photodegradation results of CECs and *E. coli* inactivation using ZnO-ALPH and TiO_2-ALPH at 200 mg L^{-1} in a 10L-CPC photoreactor. IMD and SMX degradation profiles are shown in Figure S7. The CECs degradation by both catalysts shows a similar decay that was obtained in vessel photoreactors when compared in terms of Q_{UV}, achieving nearly 40 % removal in 11–12 kJ L^{-1} for both photoreactors. These results are confirmed by the kinetics constant values (k_{CPC}) (Table S5) with a ratio k_{CPC}/k_{ves} 1, demonstrating the capability of scaling up the process from lab scale to pilot plant without diminishing the efficiency of the photocatalytic treatment.

Finally, for *E. coli* inactivation (Fig. 7b), TiO_2-ALPH performance in the CPC photoreactor achieved a similar result that in the vessel photoreactor and with similar *k* values, demonstrating that this catalyst has the same efficiency in both systems. On the other hand, ZnO-ALPH achieved total inactivation of *E. coli* in 8.2 kJ L^{-1} of Q_{UV}, with a k_{CPC} value (0.317 ± 0.014 L kJ^{-1}) which is 2 times lower in comparison with k_{VES}. While there is a reduction in the rate constant, it remained higher than that obtained with TiO_2-ALPH (0.239 ± 0.010 L kJ^{-1}), achieving total inactivation of two Q_{UV} units before. The results obtained were higher in comparison with those reported in the literature, for example, Agulló-Barceló *et al.,* [61] reported a *k* value of 0.0135 ± 0.0013 min^{-1} for naturally occurring *E. coli* in SW using a 10L-CPC photoreactor with TiO_2 (100 mg L^{-1}) under sunlight. Van Grieken *et al.,* [62] informed two kinetic decay constants (0.00056 min^{-1} and 0.00166 min^{-1}) using a bench annular reactor with a lamp (365 nm) to treat 1 L of SW. *k* value of

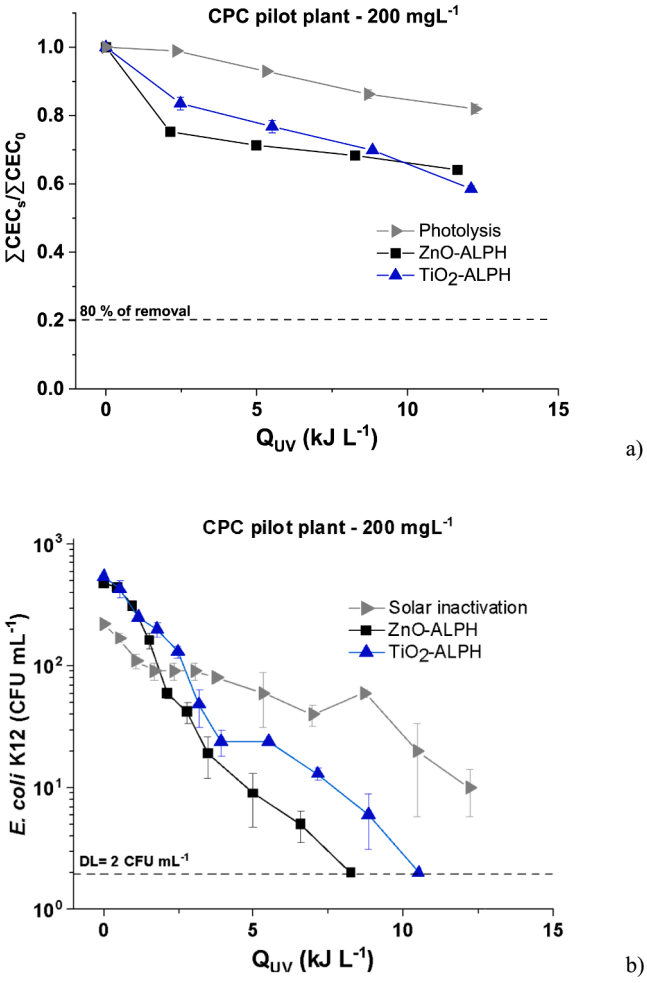


Fig. 7. Degradation of CECs (a) and inactivation of *E. coli* (b) using different catalysts at a concentration of 200 mg L^{-1} in CPC pilot plant using different catalysts SW, and under sunlight.

0.0048 min^{-1}, 0.0125 min^{-1} and 0.0033 min^{-1} in three different days has been reported by Cho *et al.* for the inactivation of *E. coli,* using a 0.6 m^2-CPC photoreactor with a concentration of TiO_2 of 100 mg L^{-1} [63]. Also, García-Fernández *et al.,* [24] achieved complete removal of *E. coli* (DL = 2 CFU mL^{-1}) in SW in 60L-CPC photoreactor with a k value of 0.025 ± 0.004 min^{-1} at 35 °C and 18.2 kJ L^{-1} of Q_{UV}, requiring twice the accumulated energy compared to ZnO-ALPH. Lastly, Rincón and Pulgarín *et al.,* [64] reported a double linear model, with $k_1 = 0.483$ min^{-1} and $k_2 = 0.300$ min^{-1} for *E. coli* at 20–25 °C in a photoreactor of 4 L with UVA lamps and 1 g L^{-1} of TiO_2, being similar to the results achieved with ZnO-ALPH. Therefore, the results indicate that both catalysts could serve as a viable alternative treatment for the disinfection and decontamination of SW.

4. Conclusions

The modified ALPH catalysts investigated in this study have shown good results for simultaneous water and wastewater decontamination and disinfection, with different performances depending on the type of additional compounds present in the ALPH structure (Fe, TiO_2 or ZnO), attributed to the photocatalytic activity.

Among the catalysts tested in DW, the best simultaneous disinfection and decontamination performance was obtained for TiO_2-ALPH catalysts (80 % of ∑CECs and > 5 LRV of *E. coli* in 45 min or 3.1 kJ L^{-1} of Q_{UV}) at the optimize catalyst concentration of 200 mg L^{-1}. Nevertheless, the higher disinfection capability (> 5 LRV in 30 min or 2.5 kJ L^{-1} of Q_{UV}) was obtained with ZnO-ALPH at 50 mg L^{-1}. On the other hand, catalysts based on iron (TiO_2-Fe-ALPH and Fe-ZnO-ALPH) showed very low photocatalytic activity. Nevertheless, these catalysts would benefit from the strategy of the addition of oxidant agents such as H_2O_2 to increase catalytic activity, options that can be matter of explore in future research. Additionally, the catalysts presented minimal leaching of iron and zinc during the treatment time.

The simultaneous SW disinfection and decontamination by ZnO-ALPH and TiO_2-ALPH, exhibited a similar photocatalytic performance trend than in DW, with a general kinetics reduction attributed to the complex water matrix composition. In comparison with commercial TiO_2, they showed similar or better efficiency, achieving 60 % of CECs removal and total inactivation of *E. coli* at 60 and 105 min of reaction for ZnO-ALPH and TiO_2-ALPH, respectively. Noteworthy also the advantages of being potentially less toxic and easily recovered, due to the significant lower water turbidity generated at the similar catalyst concentration, in comparison with TiO_2-P25.

Finally, the photocatalytic process with the best performance catalysts (TiO_2-ALPH and ZnO-ALPH) was assessed at pilot plant (CPC photoreactor) at 200 mg L^{-1}, showing similar results to the lab scale, demonstrating therefore, the potential up-scaling of these friendly-photocatalytic materials as tertiary and/or quaternary treatment, tackling wastewater regulations on reclamation and reuse. Nevertheless, further studies are required to demonstrate their photocatalytic stability for recovery and reuse.

CRediT authorship contribution statement

Jorge Castro-Rojas: Writing – original draft, Investigation, Formal analysis, Conceptualization. **María A. Rao:** Writing – review & editing, Writing – original draft, Validation, Supervision, Data curation, Conceptualization. **Ilaria Berruti:** Writing – original draft, Supervision, Investigation, Formal analysis, Data curation. **María Luz Mora:** Writing – review & editing, Validation, Supervision, Investigation, Data curation, Conceptualization. **Elizabeth Garrido-Ramírez:** Writing – review & editing, Validation, Supervision, Data curation, Conceptualization. **María Inmaculada Polo-López:** Writing – review & editing, Visualization, Validation, Supervision, Funding acquisition.

Declaration of competing interest

The authors declare that they have no known competing financial interests or personal relationships that could have appeared to influence the work reported in this paper.

Acknowledgements

The authors wish to thank the ANDROMEDA Project (PID2022-140875OB-C32) funded by MICIU/AEI/10.13039/501100011033 and the European Regional Development Fund Jorge Castro thanks the ANID/FONDECYT/11181122, ANID/FONDECYT/1230084 and the Doctoral scholarship ANID/21191833 and the Erasmus+ European Program (2020-1-IT02-KA107-078403).

Appendix A. Supplementary data

Supplementary data to this article can be found online at https://doi.org/10.1016/j.cej.2024.157894.

Data availability

Data will be made available on request.

References

[1] United Nation, United Nations Secretary-General's Plan: Water Action Decade 2018–2028, (2018). https://wateractiondecade.org/wp-content/uploads/2018/03/UN-SG- Action-Plan_Water-Action-Decade-web.pdf.
[2] M. Mofijur, M.M. Hasan, S.F. Ahmed, F. Djavanroodi, I.M.R. Fattah, A.S. Silitonga, M.A. Kalam, J.L. Zhou, T.M.Y. Khan, Advances in identifying and managing emerging contaminants in aquatic ecosystems: analytical approaches, toxicity assessment, transformation pathways, environmental fate, and remediation strategies, Environ. Pollut. 341 (2024) 122889, https://doi.org/10.1016/j.envpol.2023.122889.
[3] M. Puri, K. Gandhi, M.S. Kumar, Emerging environmental contaminants: a global perspective on policies and regulations, J. Environ. Manage. 332 (2023) 117344, https://doi.org/10.1016/j.jenvman.2023.117344.
[4] G. Reichert, S. Hilgert, S. Fuchs, J.C.R. Azevedo, Emerging contaminants and antibiotic resistance in the different environmental matrices of Latin America, Environ. Pollut. 255 (2019), https://doi.org/10.1016/j.envpol.2019.113140.
[5] M.A. Sandoval, W. Calzadilla, J. Vidal, E. Brillas, R. Salazar-González, Contaminants of emerging concern: occurrence, analytical techniques, and removal with electrochemical advanced oxidation processes with special emphasis in Latin America, Environ. Pollut. 345 (2024), https://doi.org/10.1016/j.envpol.2024.123397.
[6] G. Libralato, G. Lofrano, A. Siciliano, E. Gambino, G. Boccia, C. Federica, A. Francesco, E. Galdiero, R. Gesuele, M. Guida, Toxicity assessment of wastewater after advanced oxidation processes for emerging contaminants' degradation, Elsevier Inc. (2020), https://doi.org/10.1016/b978-0-12-818334-2.00008-0.
[7] D. Sannino, Visible light active photocatalysts for the removal of organic emerging contaminants, Elsevier Inc. (2020), https://doi.org/10.1016/b978-0-12-818334-2.00005-5.
[8] J. Castro-Rojas, P. Jofré-Dupre, N. Escalona, E. Blanco, M.S. Ureta-Zañartug, M. L. Mora, E. Garrido-ramírez, Atrazine degradation through a heterogeneous dual-effect process using Fe-TiO_2-allophane catalysts under sunlight, Heliyon. 10 (2024) e32894, https://doi.org/10.1016/j.heliyon.2024.e32894.
[9] C. Monteserín, M. Blanco, A. Juarros, A.M. Goitandia, H. Zarrabe, I. Azpitarte, E. Aranzabe, I. Espinoza-Pavón, S. Nahim-Granados, I. Berruti, M.I. Polo-López, Solar-assisted stainless-steel TiO_2-based coatings for water disinfection and decontamination, Catal. Today. 434 (2024), https://doi.org/10.1016/j.cattod.2024.114673.
[10] G. Iervolino, Visible light active photocatalysts for the removal of inorganic emerging contaminants, Elsevier Inc. (2020), https://doi.org/10.1016/b978-0-12-818334-2.00006-7.
[11] J. Castro, F. Fernández, F. Olivares, C. Berríos, E. Garrido-Ramírez, E. Blanco, N. Escalona, A. Aspée, P. Barrías, M.S. Ureta-Zañartu, Electrodes based on zeolites modified with cobalt and/or molybdenum for pesticide degradation: part II—2,4,6-trichlorophenol degradation, J. Solid State Electrochem. 25 (2021) 117–131, https://doi.org/10.1007/s10008-020-04590-6.
[12] E.G. Garrido-Ramírez, B.K.G. Theng, M.L. Mora, Clays and oxide minerals as catalysts and nanocatalysts in Fenton-like reactions - a review, Appl. Clay Sci. 47 (2010) 182–192, https://doi.org/10.1016/j.clay.2009.11.044.
[13] A.M. Méndez-Torres, J. Castro, F. Fernández, E. Garrido-Ramírez, N. Escalona, C. Gutiérrez, J.F. Marco, M. Soledad Ureta-Zañartu, Electrodes based on zeolites modified with cobalt and/or molybdenum for pesticide degradation. Part I: physicochemical characterization and efficiency of the electrodes for O_2 reduction

and H_2O_2 production, Electrocatalysis 10 (2019) 95–111, https://doi.org/10.1007/s12678-018-0500-4.
[14] H. Nishikiori, M. Furukawa, T. Fujii, Degradation of trichloroethylene using highly adsorptive allophane-TiO_2 nanocomposite, Appl. Catal. B Environ. 102 (2011) 470–474, https://doi.org/10.1016/j.apcatb.2010.12.028.
[15] E.G. Garrido-Ramírez, M.V. Sivaiah, J. Barrault, S. Valange, B.K.G. Theng, M. S. Ureta-Zañartu, M.D.L.L. Mora, Catalytic wet peroxide oxidation of phenol over iron or copper oxide-supported allophane clay materials: Influence of catalyst SiO_2/Al_2O_3 ratio, Microporous Mesoporous Mater. 162 (2012) 189–198, https://doi.org/10.1016/j.micromeso.2012.06.038.
[16] E.G. Garrido-Ramírez, M.L. Mora, J.F. Marco, M.S. Ureta-Zañartu, Characterization of nanostructured allophane clays and their use as support of iron species in a heterogeneous electro-Fenton system, Appl. Clay Sci. 86 (2013) 153–161, https://doi.org/10.1016/j.clay.2013.10.001.
[17] E.G. Garrido-Ramírez, J.F. Marco, N. Escalona, M.S. Ureta-Zañartu, Preparation and characterization of bimetallic Fe-Cu allophane nanoclays and their activity in the phenol oxidation by heterogeneous electro-Fenton reaction, Microporous Mesoporous Mater. 225 (2016) 303–311, https://doi.org/10.1016/j.micromeso.2016.01.013.
[18] S. Ohta, K. Yoshida, T. Hongo, Synthesis of allophane from rice husk ash and its use as a phosphate adsorbent: a novel approach, J. Environ. Chem. Eng. 10 (2022) 108634, https://doi.org/10.1016/j.jece.2022.108634.
[19] D. Peixoto, I. Pereira, M. Pereira-Silva, F. Veiga, M.R. Hamblin, Y. Lvov, M. Liu, A. C. Paiva-Santos, Emerging role of nanoclays in cancer research, diagnosis, and therapy, Coord. Chem. Rev. 440 (2021) 213956, https://doi.org/10.1016/j.ccr.2021.213956.
[20] Aeroxide http://www.aerosil.com/lpa-productfinder/page/productsbytext/detail.html?pid=1822&lang=en⟩ (accessed November 2024).
[21] I. Berruti, N.P.F.F. Gonçalves, P. Calza, M.C. Paganini, I. Oller, M.C. Paganini, I. Oller, M.I. Polo-López, Natural solar activation of modified zinc oxides with rare earth elements (Ce, Yb) and Fe for the simultaneous disinfection and decontamination of urban wastewater, Chemosphere 303 (2022), https://doi.org/10.1016/j.chemosphere.2022.135017.
[22] Swiss Federal Council, The Swiss Federal Council Waters Protection Ordinance (WPO), (1998). https://www.fedlex.admin.ch/eli/cc/1998/2863_2863_2863/en%0A.
[23] I. García-Fernández, S. Miralles-Cuevas, I. Oller, S. Malato, P. Fernández-Ibáñez, M. I. Polo-López, Inactivation of *E. coli* and *E. faecalis* by solar photo-Fenton with EDDS complex at neutral pH in municipal wastewater effluents, J. Hazard. Mater. 372 (2019) 85–93, https://doi.org/10.1016/j.jhazmat.2018.07.037.
[24] I. García-Fernández, I. Fernández-Calderero, M.I. Polo-López, P. Fernández-Ibáñez, Disinfection of urban effluents using solar TiO_2 photocatalysis: a study of significance of dissolved oxygen, temperature, type of microorganism and water matrix, Catal. Today. 240 (2015) 30–38, https://doi.org/10.1016/j.cattod.2014.03.026.
[25] P. Fernández-Ibáñez, C. Sichel, M.I. Polo-López, M. de Cara-García, J.C. Tello, Photocatalytic disinfection of natural well water contaminated by *Fusarium solani* using TiO_2 slurry in solar CPC photo-reactors, Catal. Today. 144 (2009) 62–68, https://doi.org/10.1016/j.cattod.2009.01.039.
[26] M.I. Polo-López, P. Fernández-Ibáñez, I. García-Fernández, I. Oller, I. Salgado-Tránsito, C. Sichel, Resistance of *Fusarium* sp spores to solar TiO_2 photocatalysis: influence of spore type and water (scaling-up results), J. Chem. Technol. Biotechnol. 85 (2010) 1038–1048, https://doi.org/10.1002/jctb.2397.
[27] E. Jeong, C.U. Kim, J. Byun, J. Lee, H.E. Kim, E.J. Kim, K.J. Choi, S.W. Hong, Quantitative evaluation of the antibacterial factors of ZnO nanorod arrays under dark conditions: physical and chemical effects on *Escherichia coli* inactivation, Sci. Total Environ. 712 (2020) 136574, https://doi.org/10.1016/j.scitotenv.2020.136574.
[28] A. Sirelkhatim, S. Mahmud, A. Seeni, N.H.M. Kaus, L.C. Ann, S.K.M. Bakhori, H. Hasan, D. Mohamad, Review on zinc oxide nanoparticles: antibacterial activity and toxicity mechanism, Nano-Micro Lett. 7 (2015) 219–242, https://doi.org/10.1007/s40820-015-0040-x.
[29] M. Zare, K. Namratha, K. Byrappa, D.M. Surendra, S. Yallappa, B. Hungund, Surfactant assisted solvothermal synthesis of ZnO nanoparticles and study of their antimicrobial and antioxidant properties, J. Mater. Sci. Technol. 34 (2018) 1035–1043, https://doi.org/10.1016/j.jmst.2017.09.014.
[30] D. Suresh, P.C. Nethravathi, M.A.P. Udayabhanu, H.R. Kumar, H. Naika, S.C. S. Nagabhushana, Chironji mediated facile green synthesis of ZnO nanoparticles and their photoluminescence, photodegradative, antimicrobial and antioxidant activities, Mater. Sci. Semicond. Process. 40 (2015) 759–765, https://doi.org/10.1016/j.mssp.2015.06.088.
[31] R.E. Núñez-Salas, J. Rodríguez-Chueca, A. Hernández-Ramírez, E. Rodríguez, M.D. L. Maya-Treviño, Evaluation of B-ZnO on photocatalytic inactivation of *Escherichia coli* and *Enterococcus* sp, J. Environ. Chem. Eng. 9 (2021), https://doi.org/10.1016/j.jece.2020.104940.
[32] WHO, Guidelines for Drinking-Water Quality, fourth ed. WHO Library Cataloguing-in-Publication, (2011). https://www.who.int/publicati ons/i/item/9789241549950.
[33] USEPA, Drinking water regulations and contaminants, (2009). https://www.epa.gov/sdwa/drinking-water-regulations-and-contaminant.
[34] K.G. McGuigan, R.M. Conroy, H.J. Mosler, M. du Preez, E. Ubomba-Jaswa, P. Fernandez-Ibañez, Solar water disinfection (SODIS): a review from bench-top to roof-top, J. Hazard. Mater. 235–236 (2012) 29–46, https://doi.org/10.1016/j.jhazmat.2012.07.053.
[35] M. Berney, H.U. Weilenmann, A. Simonetti, T. Egli, Efficacy of solar disinfection of *Escherichia coli, Shigella flexneri, Salmonella Typhimurium* and *Vibrio cholerae*, J. Appl. Microbiol. 101 (2006) 828–836, https://doi.org/10.1111/j.1365-2672.2006.02983.x.
[36] A.A.G. Moreira, P. De Lima-Neto, E.W.S. Caetano, I.L. Barroso-Neto, V.N. Freire, Computational electronic structure of the bee killer insecticide imidacloprid, New J. Chem. 40 (2016) 10353–10362, https://doi.org/10.1039/c6nj02743a.
[37] M. Calabi-Floody, J.S. Bendall, A.A. Jara, M.E. Welland, B.K.G. Theng, C. Rumpel, M. de la L. Mora, Nanoclays from an andisol: extraction, properties and carbon stabilization, Geoderma 161 (2011) 159–167, https://doi.org/10.1016/j.geoderma.2010.12.013.
[38] A.A. Jara, S. Goldberg, M.L. Mora, Studies of the surface charge of amorphous aluminosilicates using surface complexation models, J. Colloid Interface Sci. 292 (2005) 160–170, https://doi.org/10.1016/j.jcis.2005.05.083.
[39] Y. Wang, J. Wang, Z. Ding, W. Wang, J. Song, P. Li, J. Liang, Q. Fan, Light Promotes the Immobilization of U(VI) by Ferrihydrite, Molecules 27 (2022) 1–11, https://doi.org/10.3390/molecules27061859.
[40] Y. Cong, Z. Li, Y. Zhang, Q. Wang, Q. Xu, Synthesis of -Fe_2O_3/TiO_2 nanotube arrays for photoelectro-Fenton degradation of phenol, Chem. Eng. J. 191 (2012) 356–363, https://doi.org/10.1016/j.cej.2012.03.031.
[41] M.S.H. Bhuiyan, M.Y. Miah, S.C. Paul, T. Das Aka, O. Saha, M.M. Rahaman, M.J. I. Sharif, O. Habiba, M. Ashaduzzaman, Green synthesis of iron oxide nanoparticle using Carica papaya leaf extract: application for photocatalytic degradation of remazol yellow RR dye and antibacterial activity, Heliyon. 6 (2020) e04603, https://doi.org/10.1016/j.heliyon.2020.e04603.
[42] K. Anil, I. Vinod, S. Shrivastava, Photocatalytic degradation of methylene blue using ZnO and 2 % Fe – ZnO semiconductor nanomaterials synthesized by sol – gel method : a comparative study, SN Appl. Sci. (2019), https://doi.org/10.1007/s42452-019-1279-5.
[43] I. Khan, K. Saeed, N. Ali, I. Khan, B. Zhang, M. Sadiq, Heterogeneous photodegradation of industrial dyes: an insight to different mechanisms and rate affecting parameters, J. Environ. Chem. Eng. 8 (2020), https://doi.org/10.1016/j.jece.2020.104364.
[44] S. Sangare, S. Belaidi, M. Saoudi, C. Bouaziz, N. Seraghni, T. Sehili, Iron-TiO_2 pillared clay nanocomposites: eco-friendly solutions for photocatalytic removal of organic and pathogen contaminants, Inorg. Chem. Commun. 160 (2024) 111923, https://doi.org/10.1016/j.inoche.2023.111923.
[45] N. Davari, M. Farhadian, A.R.S. Nazar, M. Homayoonfal, Degradation of diphenhydramine by the photocatalysts of ZnO/Fe_2O_3 and TiO_2/Fe_2O_3 based on clinoptilolite: Structural and operational comparison, J. Environ. Chem. Eng. 5 (2017) 5707–5720, https://doi.org/10.1016/j.jece.2017.10.052.
[46] B. Szczepanik, Photocatalytic degradation of organic contaminants over clay-TiO_2 nanocomposites: a review, Appl. Clay Sci. 141 (2017) 227–239, https://doi.org/10.1016/j.clay.2017.02.029.
[47] X. Li, K. Peng, H. Chen, Z. Wang, TiO_2 nanoparticles assembled on kaolinites with different morphologies for efficient photocatalytic performance, Sci. Rep. 8 (2018) 1–11, https://doi.org/10.1038/s41598-018-29563-8.
[48] M.M. Ba-Abbad, A.A.H. Kadhum, A.B. Mohamad, M.S. Takriff, K. Sopian, Visible light photocatalytic activity of Fe^{3+}-doped ZnO nanoparticle prepared via sol-gel technique, Chemosphere 91 (2013) 1604–1611, https://doi.org/10.1016/j.chemosphere.2012.12.055.
[49] M.J. Valero-Romero, J.G. Santaclara, L. Oar-Arteta, L. van Koppen, D.Y. Osadchii, J. Gascon, F. Kapteijn, Photocatalytic properties of TiO_2 and Fe-doped TiO_2 prepared by metal organic framework-mediated synthesis, Chem. Eng. J. 360 (2019) 75–88, https://doi.org/10.1016/j.cej.2018.11.132.
[50] J. Zhu, W. Zheng, B. He, J. Zhang, M. Anpo, Characterization of Fe-TiO_2 photocatalysts synthesized by hydrothermal method and their photocatalytic reactivity for photodegradation of XRG dye diluted in water, J. Mol. Catal. A Chem. 216 (2004) 35–43, https://doi.org/10.1016/j.molcata.2004.01.008.
[51] J.J. Murcia, Visible active noble metals–structured photocatalysts for the removal of emerging contaminants, Elsevier Inc. (2020), https://doi.org/10.1016/b978-0-12-818334-2.00002-x.
[52] H. Li, W. Tu, Y. Zhou, Z. Zou, Z-scheme photocatalytic systems for promoting photocatalytic performance: recent progress and future challenges, Adv. Sci. 3 (2016), https://doi.org/10.1002/advs.201500389.
[53] V.K. Landge, S.H. Sonawane, M. Sivakumar, S.S. Sonawane, G. Uday Bhaskar Babu, G. Boczkaj, S-scheme heterojunction Bi_2O_3-ZnO/Bentonite clay composite with enhanced photocatalytic performance, Sustain. Energy Technol. Assessments. 45 (2021) 101194, https://doi.org/10.1016/j.seta.2021.101194.
[54] Z. Masood, A. Ikhlaq, U. Farooq, F. Qi, F. Javed, H. Abdul, Journal of water process engineering removal of anti-biotics from veterinary pharmaceutical wastewater using combined electroflocculation and Fe-Zn loaded zeolite 5A based catalytic ozonation process, J. Water Process Eng. 49 (2022) 103039, https://doi.org/10.1016/j.jwpe.2022.103039.
[55] N. Amini, M. Soleimani, N. Mirghaffari, Photocatalytic removal of SO2 using natural zeolite modified by TiO_2 and polyoxypropylene surfactant, Environ. Sci. Pollut. Res. 26 (2019) 16877–16886, https://doi.org/10.1007/s11356-018-1305-y.
[56] J.P. Montañez, S. Gómez, A.N. Santiago, L.B. Pierella, TiO_2 supported on HZSM-11 zeolite as efficient catalyst for the photodegradation of chlorobenzoic acids, J. Braz. Chem. Soc. 26 (2015) 1191–1200, https://doi.org/10.5935/0103-5053.20150083.
[57] Y. Zhang, H. Gan, G. Zhang, A novel mixed-phase TiO_2/kaolinite composites and their photocatalytic activity for degradation of organic contaminants, Chem. Eng. J. 172 (2011) 936–943, https://doi.org/10.1016/j.cej.2011.07.005.
[58] R.L. Parfitt, Allophane and imogolite: role in soil biogeochemical processes, Clay Miner. 44 (2009) 135–155, https://doi.org/10.1180/claymin.2009.044.1.135.

[59] M. Ozdal, S. Gurkok, Recent advances in nanoparticles as antibacterial agent, ADMET DMPK. 10 (2022) 115–129, https://doi.org/10.5599/admet.1172.
[60] C. Bogatu, M. Covei, M.I. Polo-l, A. Duta, S. Malato, Novel ZnO photocatalysts for pollutants ' abatement under solar radiation at pilot plant scale, Catal. Today 415 (2023), https://doi.org/10.1016/j.cattod.2022.11.008.
[61] M. Agulló-Barceló, M.I. Polo-López, F. Lucena, J. Jofre, P. Fernández-Ibáñez, Solar Advanced Oxidation Processes as disinfection tertiary treatments for real wastewater: implications for water reclamation, Appl. Catal. B Environ. 136–137 (2013) 341–350, https://doi.org/10.1016/j.apcatb.2013.01.069.
[62] R. van Grieken, J. Marugán, C. Sordo, C. Pablos, Comparison of the photocatalytic disinfection of *E. coli* suspensions in slurry, wall and fixed-bed reactors, Catal. Today. 144 (2009) 48–54, https://doi.org/10.1016/j.cattod.2008.11.017.
[63] I.H. Cho, I.Y. Moon, M.H. Chung, H.K. Lee, K.D. Zoh, Disinfection effects on *E. coli* using TiO_2/UV and solar light system, Water Sci Technol. Water Supply. 2 (2002) 181–190, https://doi.org/10.2166/ws.2002.0023.
[64] A.G. Rincón, C. Pulgarin, Use of coaxial photocatalytic reactor (CAPHORE) in the TiO_2 photo-assisted treatment of mixed *E. coli* and *Bacillus* sp. and bacterial community present in wastewater, Catal. Today. 101 (2005) 331–344, https://doi.org/10.1016/j.cattod.2005.03.022.